



CHORUS

This is the accepted manuscript made available via CHORUS. The article has been published as:

Microalga propels along vorticity direction in a shear flow

Anwar Chengala, Miki Hondzo, and Jian Sheng

Phys. Rev. E **87**, 052704 — Published 9 May 2013

DOI: [10.1103/PhysRevE.87.052704](https://doi.org/10.1103/PhysRevE.87.052704)

A microalga propels along vorticity direction in a shear flow

Anwar Chengala^{†‡}, Miki Hondzo[†], Jian Sheng^{‡1}

[†]St. Anthony Falls Laboratory, Department of Civil Engineering, University of Minnesota, Minneapolis, MN 55455, USA

[‡]Department of Aerospace Engineering and Mechanics, University of Minnesota, Minneapolis, MN 55455, USA

¹current affiliation: Department of Mechanical Engineering, Texas Tech University, Lubbock, Texas

Using high speed digital holographic microscopy and microfluidics, we discover that, when encountering fluid flow shear above a threshold, unicellular green alga *Dunaliella primolecta* migrates unambiguously in the cross-stream direction that is normal to the plane of shear and coincides with the local fluid flow vorticity. The flow shear drives motile microalgae to collectively migrate in a thin two-dimensional horizontal plane and consequently alters the spatial distribution of microalgal cells within a given suspension. This shear-induced algal migration differs substantially from periodic rotational motion of passive ellipsoids, known as Jeffery Orbits, as well as gyrotaxis by bottom-heavy swimming microalgae in a shear flow due to the subtle interplay between torques generated by gravity and viscous shear. Our findings could facilitate mechanistic solutions for modeling planktonic thin layers and sustainable cultivation of microalgae for human nutrition and bioenergy feedstock.

Most microalgae are motile and swim in three-dimensional (3D) complex trajectories [1] that allow them to explore and interact with the surrounding environment. Spatial gradients of environmental stimuli are known to alter microorganism swimming behavior and cause taxes [2-4] including chemotaxis, gyrotaxis, phototaxis, and rheotaxis. Insights on these directional migrations have strong implications for predator-prey interactions [1], micro-rheology of active particle suspensions [5], microorganism nutrient exploration [6], the carbon cycle [7], high-concentrations of microorganism aggregation within oceanic and lake thin layers [8], and biofuel and nutrition production by microalgae [9-10]. Although motile microorganisms encounter a diversity of fluid flow environments [11, 12], and flow affects their physiological and behavioral functions [13-16], fewer reports on shear responses [8, 16, 20, 21] have been documented. We present an experimental observation that a green alga, *Dunaliella primolecta*, responds to the flow shear by reorienting itself and swimming in the cross-stream direction normal to the plane of shear [x - z plane in Fig. 1(b)], which is also the direction of local flow vorticity [y -axis shown in Fig. 1(b)]. This migration is substantially different from the cell swimming towards or away from the oncoming flow, known as rheotaxis [17-19], as well as organisms with asymmetric shape and/or body density reorienting and swimming in the plane of shear as a result of the combined effect of gravitational and viscous forces, coined by Kessler [16] as gyrotaxis [8,16, 20]. In this paper, we demonstrate that *D. primolecta* does not behave like a passive particle in a shear flow. We will also show that this shear-induced response causes collective directional migration and alters the spatial distribution of microalgal concentration within a suspension.

D. primolecta is a bi-flagellated unicellular green alga with a body length of about 10 μm [inset in Fig. 1]. The alga is reported as neutrally buoyant [22] since it accumulates on average 23% of its body weight with lipids and is often targeted for biofuel and human nutrition production. Using microfluidics and high-speed digital holographic microscopy (DHM), we have quantified 3D swimming characteristics of *Dunaliella* in a shear flow. The experiments were conducted in a straight Polydimethylsiloxane (PDMS) micro-channel of $35 \times 3.5 \times 0.42 \text{ mm}^3$. The suspensions of *Dunaliella* were injected into the micro-channel by a computer controlled syringe pump to provide different shear stimuli ($S=du/dz$) at 0, 0.1, 1, 5, 10, and 20 s^{-1} . The obtained streamwise flow velocity distribution agreed well with the profiles of a two-dimensional (2D) Poiseuille flow [see SI Fig. S2]. A digital holographic microscopy (set up shown in SI Fig. S1 and details in [23, 30]) incorporated with a Nikon TS-100 microscope was used to image a sample volume of $760 \times 760 \times 420 \mu\text{m}^3$. An imaging objective with the magnification of 20X (Super Plan Fluor 20X) was used. The lighting was provided by a 7 mW He-Ne collimated laser (red, 0.632 μm wavelength). The wavelength of the laser was selected specifically within the range that *Dunaliella* were known to be insensitive to [31]. Additionally, to minimize the effect of phototaxis, uniform intensity of red laser lighting throughout the experimental section was provided. The original holograms were

recorded by a $2K \times 2K$ CCD camera (Imperx 4M15L) and were streamed continuously at the rate of 15 frames per second (fps) to a data acquisition computer. Each time sequence consisted of three minutes recording, totaling 1000 holograms per sequence. In-house digital reconstruction and analysis software enabled simultaneous tracking of thousands of particles located within suspensions [23]. Positions of *Dunaliella* were computed from in-focus images based on cell morphology. Microalgal swimming velocities and directions were obtained from 3D trajectories. Additional information on cell orientations (zenith angle, ϕ and azimuthal angle, θ [Fig. 3(b)]) were also generated from the in-focus images. High-speed microscopic movies at the magnification of 100X were employed to further quantify the kinematics of beating flagella and rotational motion of the cell body as well as to provide the phenomenological basis for a physical model.

In a quiescent flow, *Dunaliella* swims in a complex 3D trajectory with random body orientation [Fig. 1(a)]. While propelling forward, the cell rotates along the fore-aft axis at $\sim 2\text{Hz}$ counter clockwise, viewed from the rear of the cell body [Fig. 2(a), SI Movie **S1**, and 24, 26]. Note that *cis* (located closer to the eyespot) and *trans* (the other) flagellum of *Dunaliella* beat asynchronously [24] with occasional synchrony. Flow shear has no obvious effects on the kinematics of flagella [SI Movie **S4**]. As the fluid flow in the micro-channel exceeds a critical shear of 10 s^{-1} , *Dunaliella* **reorients** the cell body [Figs. 1(b)-1(d)] and swims in the cross-stream direction (y -axis or the spanwise flow direction) that is perpendicular to the plane of shear (x - z plane). The critical shear regions are situated close to the top and bottom walls of the micro-channel. The observed thickness is extended up to $150 \mu\text{m}$ from either wall. Close inspection of swimming directions in the critical shear regions revealed that *Dunaliella* prefer to swim in the direction of the local flow vorticity, $\omega_y = (\frac{\partial w}{\partial x} - \frac{\partial u}{\partial z})/2$. [symbols as defined in Fig. 1(b)]. In the region near the bottom wall, flow vorticity pointing in the positive y -axis corroborates with the dominant cross-stream migration direction [in-focus cell images superimposed on the x - y plane shown in Fig. 1(c)], whereas near the top the trend reverses [Fig. 1(d)]. Swimming in the negative vorticity direction is largely absent, if not completely. In the mid-section of the micro-channel where the shear is weak, cells are advected by the flow. The trajectories of these cells appear as streaks aligned in the streamwise direction, and are consequently removed from Fig. 1(b) for clarity. No vertical migration in the z -direction was observed. The diagonal trajectories shown in Figs. 1(c)-1(d) are the results of the advection in streamwise direction and cross-stream swimming in the spanwise direction. Note that in the micro-channel [Fig. 1(b)], there is no flow velocity in the direction of swimming. This cross-stream swimming in response to flow shear is robust and readily reproducible at any shear rate above the threshold [SI Movie **S2**].

In contrast to the quiescent flow, flow shear induces substantial changes in cell swimming kinematics, i.e. speed, cell body orientation and fore-aft axial rotation. In a quiescent flow, *Dunaliella* rotates about its fore-aft axis, owing to the asymmetric attachment of flagella [details in SI §4.3]. With the onset of fluid

flow shear, cells are noticeably irrotational and align themselves in the y -direction. Using high speed microscopic observations at the magnification of 100X and 1K fps, we show that a cell performing cross-stream migration *does not rotate* along its long axis [Fig. 2(b), SI Movie S2]. Note that passive ellipsoidal particles immersed in a low shear flow are driven by the flow vorticity and undergo periodic rotation [25]. It is reasonable to expect that flow shear may weaken or strengthen the rate of rotation if cell swims in or against the local vorticity direction, respectively. However, we have only observed reduction in the rate of rotation. Additionally, we have also observed that swimming *Dunaliella* behave diametrically differently from the non-motile passive particles. We have performed the same shear flow experiments on the preserved (dead) *Dunaliella* and observed that non-motile cells do undergo characteristic periodic orbital motion, as predicted by Jeffrey [25, Fig. 2(c), SI Movie S3]. Hence, it is concluded that the cell motility plays a significant role in this aberrant shear response.

To examine the alignment of the cell to shear flow, we measured the azimuthal angle, θ , and zenith angle, ϕ , defined by the cell's fore-aft axis and mean flow direction [x -axis, Fig. 3(b)]. The ϕ was estimated by the relation, $\sin(\phi) = l_{img}/l_n$, where l_{img} was the cell's fore-aft axial length measured from its projection on the in-focus image, and l_n was the nominal cell body length ($\sim 10 \mu\text{m}$). The azimuthal angle was computed as the angle between l_{img} and the flow direction (x -axis). Probability Density Functions (PDFs) of θ and ϕ were obtained for all shear rates. For brevity, only distributions of θ for $S=1 \text{ s}^{-1}$ (dashed line) and 20 s^{-1} (dark line) are shown in Fig. 3(a). Additional distribution of ϕ for 20 s^{-1} is shown in SI Fig. S6. Note that the distributions are compiled over the entire sample volume in which *Dunaliella* experienced maximum shear near the wall and minimal shear at the center of the channel. In the flow where the maximum shear is below the critical rate, 10 s^{-1} , the distributions are shown to be uniform, whereas PDFs peak at the azimuthal angle of 90° in the presence of high shear, i.e. cells are aligned in the cross-stream direction (y -axis). The PDF of cross-stream migration velocity, v , of *Dunaliella* cells at a shear rate of 20 s^{-1} [left inset in Fig. 3(a)] with advection velocity removed over the entire sample volume, shows a tri-modal distribution. The central peak located at $v=0 \pm 5 \mu\text{m s}^{-1}$ corresponds squarely to the spanwise velocity component associated with the cells advected by the flow in the low shear region ($150 < z < 300 \mu\text{m}$); whereas two side peaks (centered at $\pm 40 \mu\text{m s}^{-1}$) indicate the y -axis migration in two high shear regions close to the wall. Close inspection shows that the peak at $-40 \mu\text{m s}^{-1}$ is produced solely by the cells swimming near the top wall. Similarly, the cells near the bottom wall are associated only with the peak at $+40 \mu\text{m s}^{-1}$. Consequently, these cells located in both regions contribute to the peak in the PDF of θ at 90° [Fig. 3(a)]. The results are consistent with the abovementioned cross-stream migratory observations. To answer the question whether such a cross-stream migration is a purely hydrodynamic interaction of *Dunaliella* and a solid wall, we explore the joint PDF of the azimuthal alignment with respect to the wall distance, z [right inset of Fig. 3(a)]. Peaks of the

joint PDF (indicated by **red dark** region) protrude substantially away from the channel walls, $\sim 15 l_n$. These protrusions maintained their shape as they move away from the wall, but quickly lose their integrity to the random orientation, i.e. uniform distribution marked by green (in the mid-section of the channel). The transition from directional alignment to random is rapid and occurs sharply at the distance where the flow shear drops below the critical value. Additionally, elucidated in SI Fig. S5 [30], the cross-stream migration behavior emerges only after the flow shear exceeds 10 s^{-1} as evidenced by the tri-modal distributions of PDFs of the cross-stream velocity, v . Furthermore, the 2D high speed microscopic observations under higher shear conditions (Table S2, [30]) reveal that cross-stream migration can be observed at the plane sufficiently far away from the wall, $z = 75\sim 125 \mu\text{m}$ ($7\sim 15 l_n$). At such distances, hydrodynamic forces due to the wall are expected to be weak and often negligible [35]. These observations suggest that the cross-stream migration relate directly to the local flow shear.

Unlike a passive ellipsoid particle in a shear flow, motile *Dunaliella* cell remains irrotational. As shown in Fig. 2, a *Dunaliella* cell in a shear flow must beat its flagella to produce the necessary torque to balance the flow vorticity. To conceptualize a possible mechanism for such an action, we have developed a simple resistive force theory model to elucidate the generation of torque [shown in Figs. 3(b)-3(c)]. Similar to live *Dunaliella*, model cell has two flagella, *cis*- and *trans*-flagellum sketched in Fig. 3(b) as the left and right filament respectively. Both model flagella beat within a plane parallel to the fore-aft axis (y -axis) and are offset at a distance of d_{fg} to the center of mass. It is assumed that the beating patterns of these two flagella are identical and symmetric with respect to the y axis. The high speed measurements show that the *cis*-flagellum beats more rapidly than the *trans*-flagellum does, i.e. $\omega^{cis} > \omega^{trans}$, where ω is the beating frequency in radians and the superscript refers to the corresponding flagellum. To obtain the propulsive force on a beating flagellum at low Reynolds number limit, one can approximate this force with the drag exerted by the fluid motion relative to the filament [27]. It is noted briefly here and proved rigorously in SI §4.2 [30] that the magnitude of the net propulsive force on a flagellum increases linearly with its beating frequency. Consequently, the *cis*-flagellum that beats at higher frequency generates a larger propulsive force, $\langle F_p^{cis} \rangle$ [shown as a **longer red** arrow in Figs. 3(b)-3(c)] in comparison to the *trans*-flagellum. Since the direction of a propulsive force is determined solely by its beating patterns [30], the corresponding beating patterns by the *cis*- and *trans*-flagellum limit the directions of $\langle F_p^{cis} \rangle$ and $\langle F_p^{trans} \rangle$ to be symmetric with respect to the cell fore-aft axis. The axial component of $\langle F_p^{cis} \rangle$ and $\langle F_p^{trans} \rangle$ parallel to the swimming direction must balance the total drag force, \vec{F}_D , on the cell body. On the other hand, the normal components [**longer red** arrows in Fig. 3(c)] remain unbalanced and consequently produce a force normal to the fore-aft axis. Since it is located in a plane that is offset at d_{fg} away from the center of rotation, this force produces a counter clockwise (CCW) torque that causes the cell to rotate in CCW in a

quiescent flow when viewed from the rear [Fig. 3(b)]. In a planar shear flow above the critical shear rate, *Dunaliella* responds to shear by reorienting and swimming in the direction (y -axis) normal to the shear plane (x - z). The same torque by the beating flagella counteracts the viscous moment by the flow shear and prevents the cell from rotating in a shear flow. Illustrated in Fig. 3(c), since a drag force is also present on the flagellum in addition to the propulsive force, to generate the CCW torque in a shear flow, the net propulsive force, $\vec{F}_p^{cis} - \vec{F}_p^{trans}$, normal to the fore-aft axis must exceed the total drag force on the flagella, $\vec{F}_{df}^{cis} + \vec{F}_{df}^{trans}$. This relationship provides us with a criterion that determines the minimum frequency difference between *cis*- and *trans*-flagellum necessary to allow *Dunaliella* to maintain irrotationality in a shear flow while migrating cross stream. The criterion is provided briefly here as $\Delta f_{min} \geq S \left(\frac{2d_{fg}}{l_f} \right) C$ and more details in SI, where S is the flow shear, l_f is the length of each flagellum, and C is a coefficient that depends only on the kinematics of the beating flagella. The criterion is simple but descriptive and provides us with the lower bound. We validate this criterion against the experimental observations. For instance, assuming a beating pattern like translating rods and using physiologically relevant parameters, i.e., flagellum length, $l_f = 12 \mu\text{m}$, offset distance, $d_{fg} = 0.5 \mu\text{m}$ and a shear rate of 20 s^{-1} , the minimum frequency difference, Δf_{min} , is estimated as 2.9 Hz. The predicted value is well below experimentally observed frequency difference of 7 Hz, i.e. the beating frequency of 30 Hz for the *trans* and of 37 Hz for the *cis*-flagellum. Additional discussion are provided in SI §4 [30]. Note that this model describes one of *possible* mechanisms that may explain the two primary experimental observations: (i) In the presence of flow shear above a critical value, motile *Dunaliella* reorients itself and swims in the direction of local flow vorticity; and (ii) *Dunaliella* is capable of maintaining the cell body irrotational in a shear flow, whereas in quiescent fluid, it rotates about its fore-aft axis while swimming forward. The other possible mechanisms may include but are not limited to: both flagella beat in three dimensions and are not confined within a single 2D plane, or *trans*- and *cis*-flagella could beat in different planes. To discern which mechanism is involved, our observations may not be sufficient to explain the full scope. Further research will be needed.

To assess the implications of the aforementioned shear-induced response for large-scale biophysical processes, we compute both isotropic and anisotropic dispersion coefficients [30, SI in 23, Figs. 4(a) and 4(b)]. To determine the swimming induced dispersion coefficients (D_{ii} , $i = x, y, z$), we apply the Lagrangian description of diffusion, which has been introduced by Taylor [32] to determine the dispersion rate of a scalar in stationary, homogeneous, and isotropic turbulence, subsequently extended by Csanady [33] to suspended particles, and employed to swimming micro-organisms by Sheng *et al.* [23]. It

is shown that the dispersion coefficient can be calculated by integrating the autocorrelation function, $R_{ii}(\tau)$, of the Lagrangian velocity components along the particle trajectory, i.e.,

$$D_{ii}(t) = \int_0^t R_{ii}(\tau) d\tau = \int_{\tau=0}^t \int_{\eta=0}^{\infty} u_i(\eta) u_i(\eta + \tau) d\eta d\tau$$

where τ is the time lag, u is the fluctuation component of *Dunaliella* swimming velocity, and the subscript i refers to a direction, x , y or z . Due to the limited spatial extent of essentially all velocity measurement, the dispersion coefficient is ensemble averaged over many microalgal trajectories with a finite length as,

$$D_{ii}(t) = \left\langle \int_0^t d\tau \int_0^\tau R_{ii}(\eta) d\eta \right\rangle = \int_0^t d\tau \int_0^\tau \langle R_{ii}(\eta) \rangle d\eta$$

where $\langle \rangle$ denotes ensemble averaging performed over trajectories of *Dunaliella*. The asymptotic value of $D_{ii}(\tau)$, as $\tau \rightarrow \infty$, yields the Fickian dispersion coefficient. The isotropic dispersion, D , is estimated by averaging the coefficient, $D = \frac{1}{3}(D_{xx} + D_{yy} + D_{zz})$. The subsequent anisotropic dispersion rate is computed by $A_{ii} = \left(\frac{D_{ii}}{D}\right) - 1$. The value of A_{ii} indicates the extent of anisotropy in the i -th direction. A positive A_{ii} suggests that in the i -th direction *Dunaliella* disperse faster than the isotropic rate. To elucidate visually the effects of the abovementioned cross-stream migration on dispersion, we have plotted swimming trajectories at two flow conditions ($S = 0 \text{ s}^{-1}$ and $S = 20 \text{ s}^{-1}$) [Fig. 4(c)]. Each trajectory is made to originate from the same point and color-coded by the time as *Dunaliella* disperses. The suspension disperses less in the presence of low flow shear than it does in quiescent fluid, whereas the dispersion increases “exponentially” as shear is increased. The initial reduction in dispersion are consistent with the observations by Chengala et al [34] that *Dunaliella* reduce the swimming velocity while acclimatizing to the low shear flow conditions. Further, the disparity among the components of anisotropic dispersion tensor shows the structural change of the suspension as it diffuses. At no or low shear ($S < 5 \text{ s}^{-1}$), suspension diffuses nearly uniformly in all directions [Top in Fig. 4(c)]. In the regime, $5 < S < 10 \text{ s}^{-1}$, *Dunaliella* prefer to swim axisymmetrically in the direction of mean flow. As the shear increases to induce the aforementioned response, the population disperses in a 2D plane perpendicular to shear [bottom in Fig. 4(c)].

In conclusion, we observe that a green alga, *D. primolecta*, aligns and swims in a preferred direction at the flow shear above the critical rate of 10 s^{-1} . The resultant swimming direction is perpendicular to the shear plane (x - z) and in-line with local vorticity (y -axis), and is substantially different from that of gyrotaxis: a phenomenon occurring due to asymmetric distribution of cell mass or bottom heaviness, where the cells reorient by the subtle balances between gravitation and viscous torques. The cells must

swim vertically and the plane of shear must align vertically. In contrast, in our quiescent flow experiments, *D. primolecta* swim in random directions, which are evident in PDFs of cell orientations [Fig. 3(a)] and 3D trajectories [Fig. 1(a), Fig. 4(c)]. In high shear experiments, we observe that *Dunaliella* prefers swimming on horizontal planes (x - y planes) normal to the shear (x - z). It is evident in the PDF distribution shown in SI Fig. S5 for zenith angle, ϕ , compiled over 1000 sample tracks where the PDF peaks at $\cos(\phi) = 0^\circ$ or $\phi = 90^\circ$. In contrast to the motion of an elongated passive particle in a shear flow, the cell body of *Dunaliella* remains irrotational. This active shear-induced response results in a substantial change in spatial heterogeneity of microalgal suspension, forming what appears to be a 2D thin dispersion layer. Note that the y -axis overlaps with the intermediate strain of a planar shear in which direction cells experience the least net stress on the membrane. The discovery motivates an interesting paradigm to harvest microalgae at large scales from diluted bioreactors by manipulating hydrodynamic cues. Microalgal biomass separation from dilute suspensions is one of the highest energy costs associated with biofuels and human nutrition production. The observed shear-induced swimming provides additional insights into the mechanisms and processes that mediate the formation, maintenance, and dispersion of microalgal thin layers in lakes and oceans.

JS has been supported by an NSF CAREER Award (No: CBET-0844647) and NSF grant (No: DBI-0852875), AC and MH have been partially supported by NSF (No EAR-0120914) grant. Additional support is provided by the Minnesota Futures Grant, University of Minnesota, to MH.

1. J. Sheng, E. Malkiel, J. Katz, J. Adolf, R. Belas and A. R Place, Proc. Natl. Acad. Sci. USA **104**, 17512 (2007).
2. T.J. Pedley and J.O. Kessler, Annu. Rev. Fluid. Mech. **24**, 313 (1992).
3. T. Fenchel, Science **296**, 1068 (2002).
4. T. Kiorboe and G.A. Jackson, Limnol. Oceanogr. **46**, 1309 (2001).
5. S. Rafai, L. Jibuti and P. Peyla, Phys. Rev. Lett. **104**, 098102 (2010).
6. N. Blackburn, T. Fenchel and J. Mitchell, Science **282**, 2254 (1998).
7. A.R. Longhurst, Limnol. Oceanogr. **36**, 1507 (1991).
8. W. M. Durham, J.O. Kessler and R. Stocker, Science **323**, 1067 (2009).
9. R. J. Wijffels and M. J. Barbosa, Science **329**, 796 (2010).
10. A. Sing, P.S. Nigam and J.D. Murphy, Bioresour. Technol. **102**, 26 (2011).
11. P.H. LeBlond and L. A. Mysak, *Waves in the ocean* (Elsevier, Amsterdam, The Netherlands, 1978).
12. M.M. Deksheniaks, P. L. Donaghay, J. M. Sullivan, J. E. B. Rines, T. R. Osborn and M. S. Twardowski, Mar. Ecol. Prog. Ser. **23**, 61 (2001).
13. M. A. R. Koehl, P. A. Jumars, and L. Karp-Boss, in *Out of the past*, edited by A.D. Norton (Brit Phycol. Assoc, Belfast, UK, 2003), p. 115.
14. M.M. Estrada and E. Berdalet, in *Phytoplankton in a turbulent world*, Lectures on plankton and turbulence, edited by C. Marrase, E. Siez, J.M. Redondo (Sci. Mar. 61 Supl. 1) p. 125.
15. F. Peters and C. Marrasé, Mar. Ecol. Prog. Ser. **205**, 291 (2000).
16. J.O. Kessler, Nature **313**, 218 (1985).
17. J.C. Montgomery, C.F. Baker, A.G. Carton, Nature **389**, 960 (1997).
18. F.P. Bretherton, and Lord F.R.S. Rothschild, R. Soc. London **153**, 490 (1961).

19. J. Hill, O. Kalkanci, J.L. McMurry and H. Koser, *Phys. Rev. Lett.* **98**, 068101 (2007).
20. T. J. Pedley and J.O. Kessler, *Annu. Rev. Fluid Mech.* **24**, 313 (1992).
21. Marcos, H. C. Fu, T. R. Powers and R. Stocker, *Proc. Natl. Acad. Sci. USA* **109**, 4780 (2012).
22. L.J. Borowitzka and M.A. Borowitzka, in *Biotechnology of Vitamins, pigments, and growth factors*, Edited by E.J. Vandamme (Elsevier, NY, USA, 1989), p 22.
23. J. Sheng, E. Malkiel, J. Katz, J. Adolf, R. Belas and A. R Place, *Proc. Natl. Acad. Sci. USA* **107**, 2082 (2010).
24. D. Schoevaert, S. Krishnaswamy, M. Couturier, and F. Marano, *Biol. Cell.* **62**, 229 (1988).
25. G.B. Jeffery, *Proc. R. Soc. London* **102**,161 (1922).
26. R. Vismara, F. Verni, L. Barsanti, V. Evangelista and P. Gualtieri, *Micron.* **35**, 337 (2004).
27. J. Gray, and G.J. Hancock, *J. Exp. Biol.* **32**, 802 (1955).
28. J. Olmos, J. Paniagua and R. Contreras, *Lett. Appl. Microbiol.* **30**, 80 (2000).
29. J. Sheng, E. Malkiel and J. Katz, *Appl. Opt.* **45**, 3893 (2006).
30. See Supplemental Material at [URL will be inserted by publisher] for [give brief description of material]
31. K.W. Foster and R.D. Smyth, *Microbiol. Rev.* **44**, 572 (1980).
32. G. I. Taylor, *Proc. London Math. Soc.* **2**, 196 (1921).
33. G. T. Csanady, *J. Atmos. Sci.* **20**, 201 (1963).
34. A.A. Chengala, M. Hondzo, D. Troolin and P. Lefebvre, *Biotechnol. and Bioeng.* **107**, 65 (2010).
35. J. R. C. Blake and A. T Chwang, *J. Eng. Math.* **8**, 23 (1974).

Figure Legends:

Fig. 1 (Color). 3D swimming trajectories of *D. primolecta* **(a)** in a quiescent fluid, **(b)** in shear flow of $S = 20 \text{ s}^{-1}$. x : streamwise and mean flow direction, y : spanwise and the intermediate strain direction of a planar shear flow. Local vorticity aligns in the positive y axis within the bottom boundary layer and in the negative y axis within the top boundary layer. z : the wall normal direction. The cells in the mid-section of channel are advected (they appear as straight lines) and are removed to make the viewing clear. The velocity components in the corresponding direction are denoted as u , v , and w . A straight micro-channel with the rectangular cross-section of $0.42 \times 3.5 \text{ mm}^2$ is used for visualization. The trajectories are color coded by the magnitude of swimming velocity. Superimposed in-focus images of individual *Dunaliella* subjected to the high flow shear located in **(c)** bottom and **(d)** top boundary layers. Local vorticity is marked with an arrow separately. Inset - **Top**: Optical microscopic image, **Bottom**: In-focus digital holographic image of *D. primolecta*. Scale: $10 \text{ }\mu\text{m}$. Note: The diagonal trajectories shown in Figs. 1(c)-1(d) are the results of the streamwise flow advection and cross-stream swimming in spanwise.

Fig. 2 (Color Online). Sample of time sequences (only shown for every 63 frames): motile cell swims **(a)** in a quiescent fluid; **(b)** in a shear flow of $S = 20 \text{ s}^{-1}$. In a quiescent flow, cell body rotates counter clockwise about 2Hz when viewed from the rear. Rotation direction is indicated by the position of the cell nucleus with nucleolus (dark spots on the front side of the cell). In a shear flow, the cell remains irrotational and swims perpendicular to the mean flow (y -axis). **(c)** Non-motile cell (fixed with 4% formaldehyde) in a shear flow undergoes periodic motion (Jeffery Orbits, [26]). Scale: $10 \text{ }\mu\text{m}$. The figure elucidates the rotationality/non-rotationality of the cell in different fluid flow conditions. The x positions of the cell in Fig. 2(b) are, however, manually arranged closer to each other.

Fig. 3 (Color Online). **(a)** PDFs of cell alignment in a shear flow. The alignment is defined as the angle between the cell's fore-aft axis and the mean flow direction, x . Insets: Left - histogram of spanwise swimming velocity, Right - Joint PDF of θ (azimuth angle) with respect to varying micro-channel depth, and consequently flow shear. **(b)** Schematics of cell alignment in a flow: θ (azimuth angle) varies from $0 - 180^\circ$ and $\theta = 90^\circ$ represents the direction perpendicular to the flow and the direction of local vorticity. ϕ represents the zenith angle. **(c)** Hydrodynamic model of the cell in a shear flow: viscous torque by the flow is balanced by that produced by the flagella.

Fig. 4 (Color). Swimming induced dispersion **(a)** Isotropic dispersion coefficient, $D = \frac{1}{3}(D_{xx} + D_{yy} + D_{zz})$, normalized by kinematic viscosity, ν . An average error is estimated at $0.3 \times 10^{-2} \text{ }\mu\text{m}^2 \text{ s}^{-1}$ **(b)** Anisotropic dispersion tensor, $\frac{D_{ii}}{D} - 1$. Symbols: Black - D_{xx} , Red - D_{yy} , Blue - D_{zz} . The error: 0.3, 0.2,

and $0.15 \mu\text{m}^2 \text{s}^{-1}$ for D_{xx} , D_{yy} and D_{zz} , respectively. **(c)** 3D elucidation of the cell dispersion pattern using Lagrangian trajectories. All trajectories are made to originate from the same point. **Top**: a quiescent flow; **Bottom**: a shear flow of 20s^{-1} . **Color**: time elapsed.

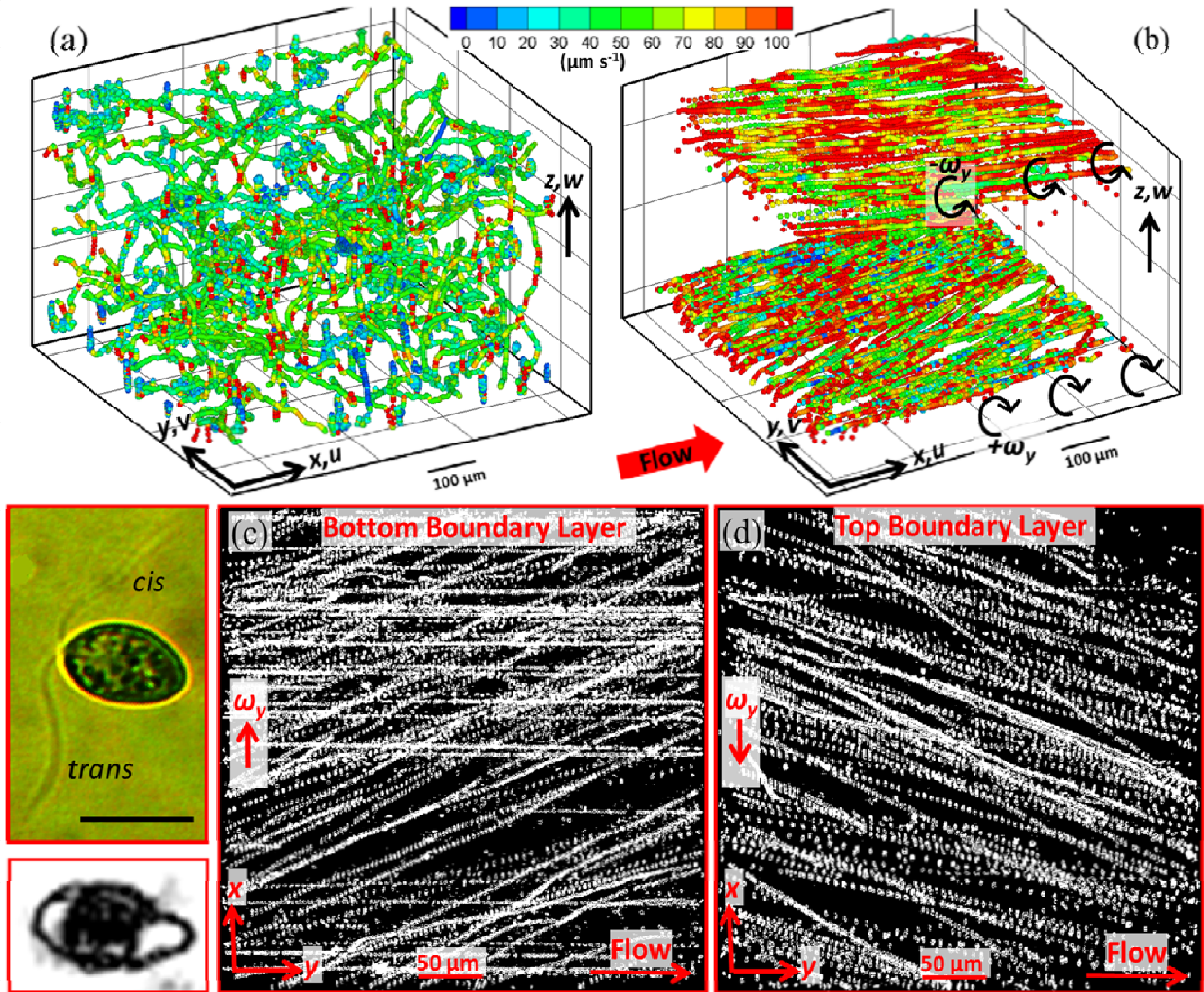


Fig. 1

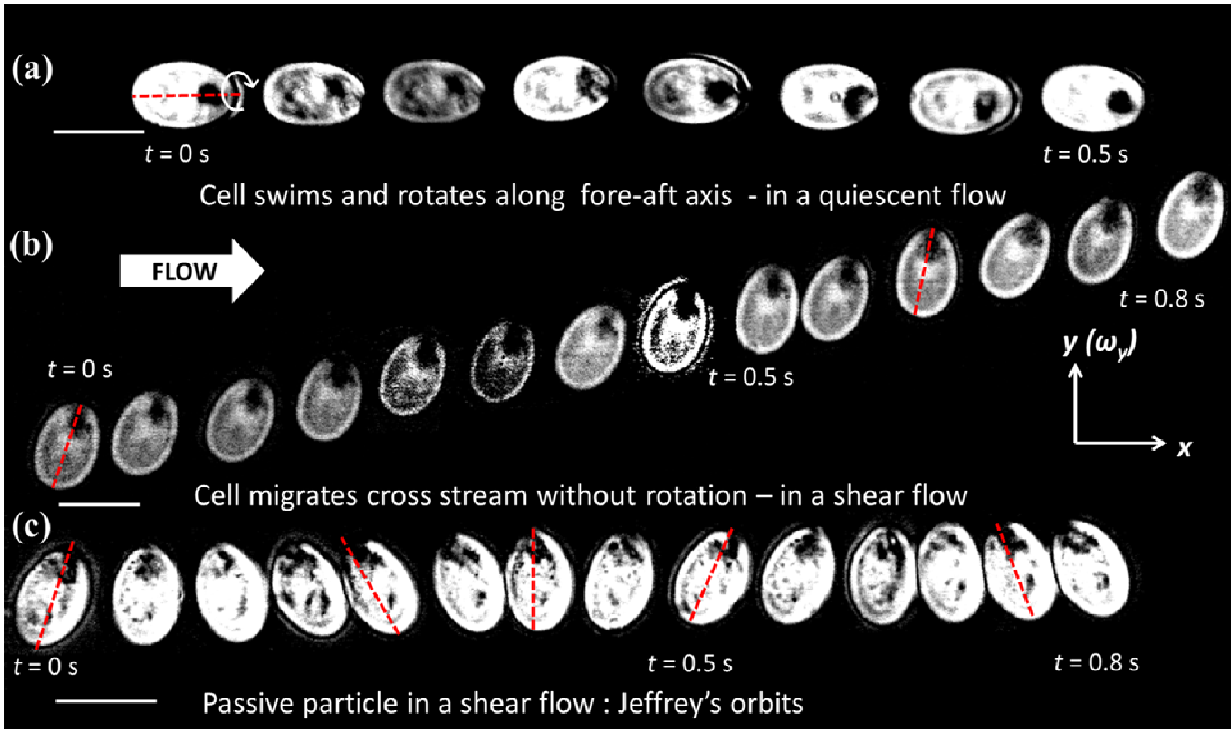


Fig. 2

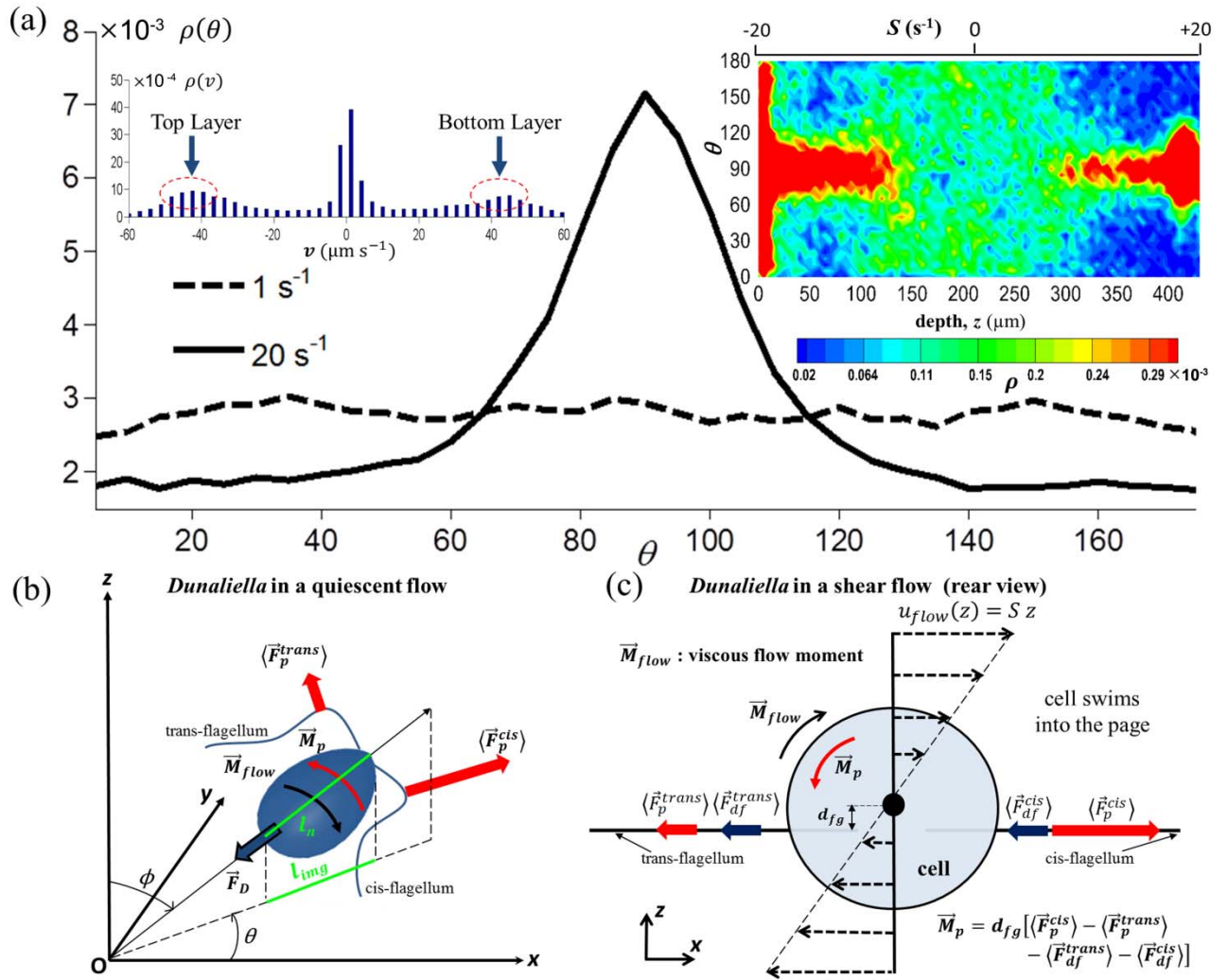


Fig. 3

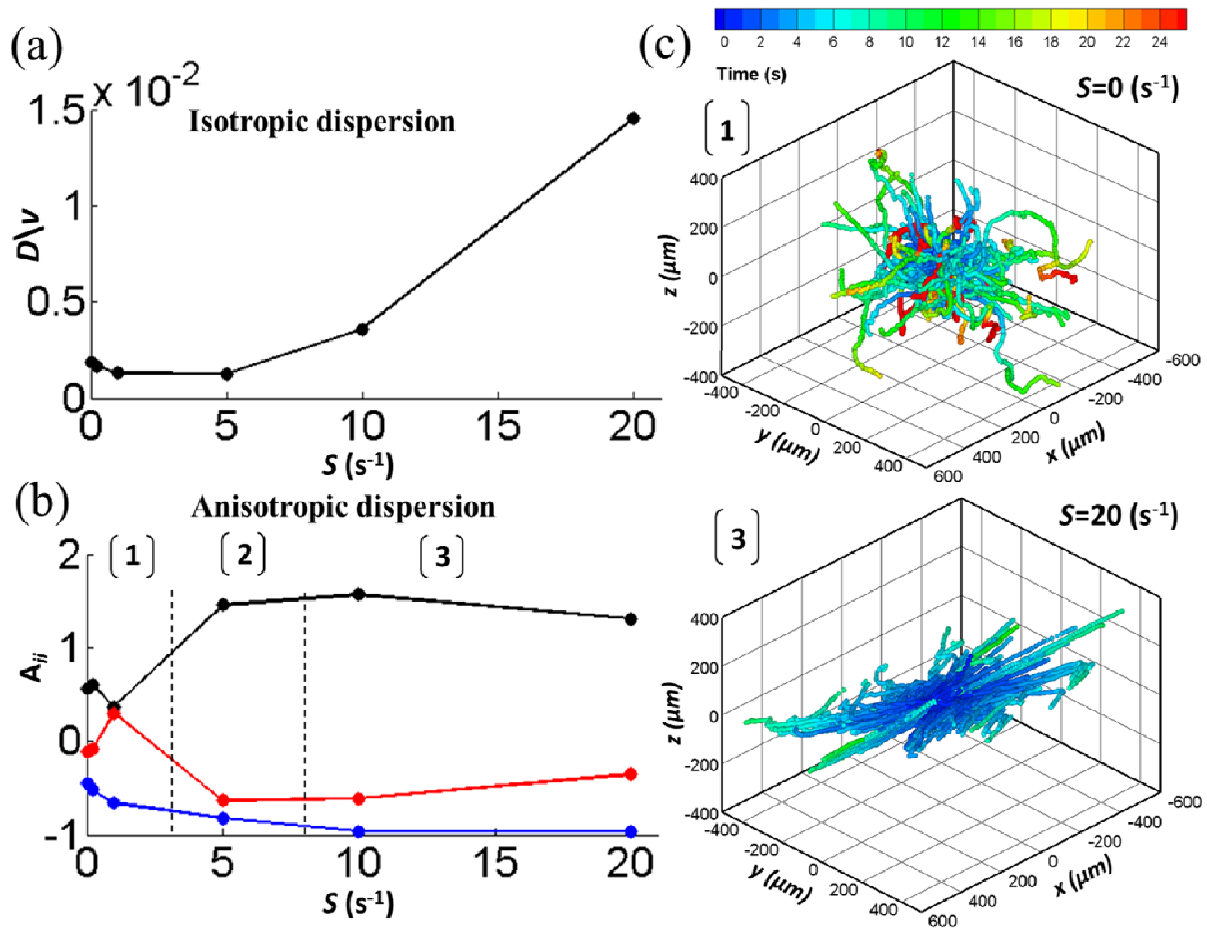


Fig. 4